separations

Article

An Empirical Investigation on the Influence of the Number of Particle Outlets and Volume Flow Rates on Separation Efficiency and Pressure Drop in a Uniflow Hydrocyclone

Thomas Senfter, Jonas Ennemoser, Manuel Berger *, Christian Mayerl, Tobias Kofler and Martin Pillei

Environmental Process & Energy Engineering Department, MCI—The Entrepreneurial School, Universitätsstraße 15, 6020 Innsbruck, Austria
* Correspondence: manuel.berger@mci.edu

Abstract: The influence of the number of particle outlets as well as of varying inlet and underflow volume flow rates on separation efficiency and pressure drop of uniflow hydrocyclones was empirically investigated. Therefore, several prototypes were designed and constructed, and separation tests were systematically conducted on a test rig. With regard to the number of particle outlets, the influence of a single, twofold and fourfold particle outlet on the separator's performance was evaluated. The results showed that a higher number of particle outlets had neither a measurable influence on the separator's separation efficiency nor on the pressure drop. However, high inlet volume flow rates favor particle separation but also lead to higher pressure drops. Accordingly, separation efficiencies in a range of 26.92 % to 38.56 % were recorded, while the pressure drop simultaneously varied between 0.218 bar and 0.413 bar. The separation efficiency was additionally enhanced by applying higher underflow volume flow rates. Increasing the underflow to inlet volume flow ratio by 4 % led to performance improvements by more than 6 % on average.

Keywords: solid–liquid separation; uniflow hydrocyclone; performance evaluation

Citation: Senfter, T.; Ennemoser, J.; Berger, M.; Mayerl, C.; Kofler, T.; Pillei, M. An Empirical Investigation on the Influence of the Number of Particle Outlets and Volume Flow Rates on Separation Efficiency and Pressure Drop in a Uniflow Hydrocyclone. *Separations* **2023**, *10*, 169. https://doi.org/10.3390/separations10030169

Academic Editor: Sohrab Zendehboudi

Received: 23 January 2023
Revised: 9 February 2023
Accepted: 28 February 2023
Published: 2 March 2023

1. Introduction

The separation of particles from fluid suspensions is an integral part of mechanical process engineering. For this purpose, the industry demands efficient and cost-effective separators that ensure a reliable operation. To meet these demands and to comply with the increasingly stringent legal requirements, a variety of factors must be considered in the design and selection of a proper separator [1,2]. Uniflow hydrocyclones are centrifugal separators which combine a variety of industrially desired properties. They consist of four main components, namely swirl vane inlet (SVI), separation chamber (SC), vortex finder (VF) and particle outlet (PO). The suspension axially enters the separator through the SVI, which consists of swirl vanes that are attached to a core. The arrangement of the swirl vanes forces the incoming suspension onto a helixual path. Within the SC, the particles are subjected to centrifugal forces, wherefore the particles are centrifuged to the wall and hence separated. While the separated particles are discharged through the PO (underflow), the purified fluid leaves the separator through the vortex finder in the overflow. Their simple, robust and compact design offers a high mechanical integrity and allows their installation in existing pipelines. Additionally, unlike conventional reverse flow hydrocyclones, uniflow hydrocyclones are characterized by a linear flow without flow reversal, which results in low pressure drops and, consequently, in energy demands [3–6]. However, despite the advantageous properties of uniflow hydrocyclones, information about their performance is still scarce and researchers mainly focused on gas–solid [4,6–9], respectively, fluid–fluid [10–15] separation using the principle of uniflow cyclones.

In the field of uniflow hydrocyclones, the first reference can be traced back to Sineath's fixed impeller hydrocyclone in 1955 [16,17]. Sineath empirically evaluated the influence of

geometric and operating parameters on the separator's performance, whereby the design of the impeller guide vanes as well as the length of the separation chamber as decisive performance-influencing parameters were identified. Additionally, it was shown that the separation efficiency decreased with increasing VF diameters as well as at high particle loadings, while higher mass flow rates led to lower separation points. Based on these insights, Sineath finally succeeded in developing a model equation, which allows one to predict the cut size diameter as a function of the mass flow rate, the VF diameter and the solid–liquid density difference of his fixed impeller hydrocyclone for a broad application range. Nonetheless, despite the efforts made by Sineath, scientists have not further processed the results in the upcoming years.

Only since 2000 have researchers independently focused on understanding and improving knowledge about the separation mechanisms of uniflow hydrocyclones through theoretical [18], experimental [19,20] and numerical [5,19,21–23] approaches. However, mostly uniflow hydrocyclones with tangential inlets were considered, which makes them less appealing for installing them in existing pipelines. Industrially desired uniflow hydrocyclones with axial inlets have been studied by Senn et al. [24] in 2018. Based on the insights from the field of gas–solid separation [6,25], Senn et al. [24] investigated the effects of variations of the SVI angles, the length and design of the SC as well as of the VF dimensions on the performance of uniflow hydrocyclones. The results showed a percentage increase of 44% in separation efficiency by decreasing the SVI angle from 15° to 45° with respect to the horizontal axis. In addition to that, the performance reached its optimum at ratios of separation chamber length to diameter between 3 to 3.5, which is related to the formation of the vortex flow. In the numerical investigations of Mokni et al. [23], an increase in separation efficiency up to a separation length to diameter ratio of 6.15 could even be observed. Additionally, Senn et al. [24] observed performance improvements as the separation chamber tapered conically towards the bottom, which was proven via numerical investigations. Regarding the VF dimensions, an ideal VF to cyclone diameter ratio of 0.57 was documented. Nonetheless, the influence of geometric and operating parameters on the performance of uniflow hydrocyclones is still not understood and the lack of generally valid design criteria still limits their industrial application up to now.

To increase the future potential of uniflow hydrocyclones, this study aims to empirically evaluate the influence of the number of particle outlets on separation efficiency and pressure drop of uniflow hydrocyclones. Additionally, the influence of varying volume flow rates will be investigated, which has already been extensively studied for conventional reverse-flow hydrocyclones (see e.g., Senfter [26], Zhang et al. [27] and Cui et al. [28]). For this purpose, three uniflow hydrocyclone prototypes are designed, constructed and manufactured such that systematic separation tests can then be conducted at a test facility.

2. Materials and Methods

To assess the performance of uniflow hydrocyclones, dispersed particles are to be separated from the continuous water phase, which maintains a constant temperature of 20 °C. Carolith 0–0.2 particles with a particle density of 2700 kg·m^{-3} and a median diameter d_{50} of 66.15 µm (d_{10} = 6.21 µm and d_{90} = 197.10 µm) are used as the disperse phase for the separation tests. Carolith 0–0.2 are test particles with a low abrasiveness, preventing wear of the separator equipment. Additionally, Carolith 0–0.2 does not dissolve in water and is hence suitable for solid–liquid separation tests. The particle size distribution of the test particles given in Figure A1 in the Appendix A is measured using the principle of laser diffraction with a Malvern® Mastersizer 2000.

2.1. Test Rig

The operation mode for the separation tests is described on the basis of the simplified piping and instrumentation diagram (P&ID) of the test rig shown in Figure 1. From the storage tank, the water reaches the circulation pump (Pump 1). The volume flow rate is set via the LabView® software and regulated by means of the flow sensor FIC 1. As a

stationary volume flow rate establishes, 0.1 kg of test particles is added to the water by means of a motor driven piston unit. In order to ensure a constant particle concentration of c_1 = 0.5 kg·m^{-3} at the inlet of the separator, the feed rate of the piston is set with a potentiometer. The suspension then reaches the uniflow hydrocyclone HC (see Figure 2 and Table 1), where particle separation takes place. For measuring the masses of the respective particle fractions, bag filter systems are implemented in the overflow and underflow ducts. The bag filters Filter 1 and Filter 2 are capable for removing particles with $d_p > 0.5$ µm, which guarantees a particle retention of 100% considering the test particles used in the experimental investigations. The purified water with fine particles as a disperse phase leaves the uniflow hydrocyclone in the overflow, where the remaining particles are collected by Filter 1 and the pure water is recirculated into the storage tank. For controlling the volume flow rate in the underflow duct, an underflow pump (Pump 2) is installed, whose volume flow rate is again set using LabView® and controlled with the flow sensor FIC 2. The separated particles are collected by Filter 2 and the particle-free water is then returned to the storage tank, closing the water circuit. The uniflow hydrocyclone's pressure drop results from the pressure difference between the main duct and the overflow duct and is recorded via the pressure indicators PI 1 and PI 2. Since the process control system records the volume flow rates and pressures every second, the pressure drop is determined with the stored data from LabView®.

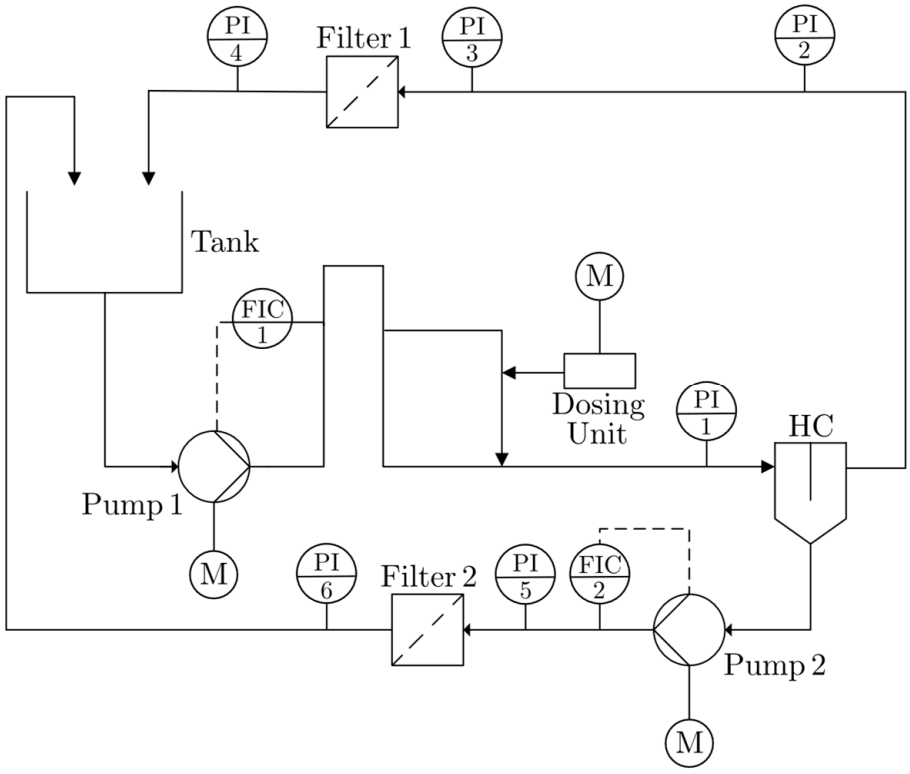

Figure 1. Simplified piping and instrumentation diagram (P&ID) of the test rig for the empirical investigations. The flow rate of pump 1 is 12, 15 or 18 m^3·h^{-1}. 0.5 kg·m^{-3} Carolith 0–0.2 is added by the dosing unit. The hydrocyclone structure and the dimensions are shown in Figure 2 and Table 1. The overflow and underflow are filtered and pump back to the tank. M: motor, FIC: flow sensor, PI: pressure indicator, HC: hydrocyclone. The used flow indicators respectively pressure indicators are identical, wherefore the labelling of the flow sensors (FIC 1 to FIC 2) and the pressure indicators (PI 1 to PI 6) follow a chronological structure.

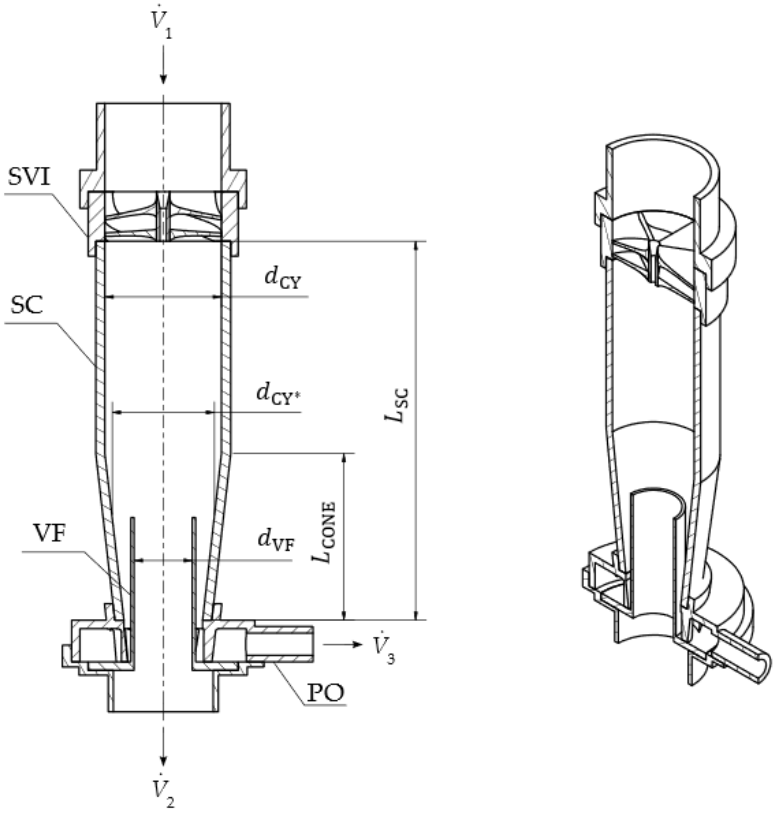

Figure 2. Exemplary uniflow hydrocyclone prototype with characteristic dimensions. SVI: swirl vane inlet, SC: separation chamber, VF: vortex finder, PO: particle outlet, d_{VF}: diameter vortex finder, d_{CY^*}, d_{CY}: cyclone diameters, L_{CONE}: length of the cone, L_{SC}: length of the separation chamber. For dimensions see text and Table 1.

Table 1. Overview of the geometric parameters of the uniflow hydrocyclone prototype.

Description	Variable	Value	Unit
swirl vane inlet angle	α_{SVI}	15	°
cyclone diameter	d_{CY}	70	mm
length of the separation chamber	L_{SC}	227.5	mm
ratio of cone length to total separation chamber length	L_{CONE}/L_{SC}	0.53	-
cone angle	β	5.4	°
ratio of vortex finder length to separation chamber length	L_{VF}/L_{SC}	0.38	-
ratio of vortex finder diameter to cyclone diameter	d_{VF}/d_{CY}	0.48	-
ratio of cyclone diameter at the location of the vortex finder to cyclone diameter	d_{CY^*}/d_{CY}	0.84	-

2.2. Dosing Unit Setting and Inlet Concentration Adjustment

As previously introduced in the description of the test rig in Section 2.1., the Carolith 0–0.2 test dust is added to the water by means of a motor driven piston unit (schematically shown in Figure A2 in the Appendix A), whose feed rate is set using a potentiometer. Since the particle concentration in the inlet of the uniflow hydrocyclone c_1 is set to be constant with a value of 0.5 kg·m^{-3} for all experimental investigations, the feed rate of the dosing unit needs to be adapted to the inlet volume flow rate $\dot{V}_1$. To do so, the dosing pipe is filled with 0.1 kg of particles (m_{feed}) in each test run. The time required for adding the particles into the continuous water phase at different potentiometer settings is then measured with a timer, which allows one to determine the mass flow rate of particle dosing $\dot{m}_{DOSING}$

according to Equation (1), where the calculation is exemplarily outlined for a potentiometer setting of 50.

$$\dot{m}_{\mathrm{DOSING,Pot\ 50}} = \frac{m_{\mathrm{feed}}}{t_{\mathrm{DOSING}}} = \frac{0.1\ \mathrm{kg}}{336\ \mathrm{s}} = 2.98{\cdot}10^{-4}\ \mathrm{kg{\cdot}s^{-1}} \tag{1}$$

Knowing the mass flow rate of particle dosing, the particle inlet concentration c_1 can be calculated according to Equation (2). Considering an exemplary inlet volume flow rate of 15 $\mathrm{m^3{\cdot}h^{-1}}$, the inlet concentration yields 0.07 $\mathrm{kg{\cdot}m^{-3}}$. Hence, the procedure is repeated by increasing the potentiometer setting in steps of 50 until the inlet concentration approaches a value of 0.5 $\mathrm{kg{\cdot}m^{-3}}$.

$$c_{1,\mathrm{Pot\ 50}} = \frac{\dot{m}_{\mathrm{DOSING,Pot\ 50}}}{\dot{V}_1} = \frac{2.98{\cdot}10^{-4}\ \mathrm{kg{\cdot}s^{-1}}}{\frac{15}{3600}\ \mathrm{m^3{\cdot}s^{-1}}} = 0.07\ \mathrm{kg{\cdot}m^{-3}} \tag{2}$$

For an inlet volume flow rate of 15 $\mathrm{m^3{\cdot}h^{-1}}$ an inlet concentration of 0.5 $\mathrm{kg{\cdot}m^{-3}}$ is obtained at a potentiometer setting between 400 and 450. Since the relationship between the potentiometer setting and the inlet concentration can be approximated using a linear function, the final potentiometer setting is ultimately determined through a linear interpolation. To find the ideal potentiometer setting, the steps explained above are repeated for all inlet volume flow rates of interest. The potentiometer setting dependent inlet concentrations of the three different volume flow rates are graphically shown in Figure A3 in Appendix A.

2.3. Performance Evaluation

Separation efficiency η_{HC} and pressure drop Δp_{HC} are specified as the uniflow hydrocyclone's performance parameters. While the pressure drop is measured via differential pressure sensors (Equation (3)), the separation efficiency is determined through the mass of test particles on the filters gravimetrically (Equation (4)).

$$\Delta p_{\mathrm{HC}} = p_{\mathrm{PI\ 1}} - p_{\mathrm{PI\ 2}} \tag{3}$$

$$\eta_{\mathrm{HC}} = \frac{m_{\mathrm{Filter\ 2}}}{m_{\mathrm{Filter\ 2}} + m_{\mathrm{Filter\ 1}}} \tag{4}$$

To check the reproducibility of the separation tests, the experiments are repeated three times for each configuration. The experiments are invalid if the separation efficiencies of the three repetitions differ more than 1.5% or if the deviation of the sum of masses of retained and separated particles of an individual experiment exceeds a tolerance range of 2%. Due to a lack of guidance in the field of solid–liquid separation, the tolerance ranges of $m_{\mathrm{Feed}} \pm 2\%$ are defined in accordance with the ISO 5011 standard [29], which refers to the separation of solids from gases.

2.4. Prototype Design and Experimental Investigations

The uniflow hydrocyclones prototypes are designed with a diameter d_{CY} of 70 mm, a swirl vane inlet angle α_{SVI} of 15° and a separation chamber length L_{SC} of 227.5 mm. Senn et al. [24] showed that the separator's performance is improved if the separation chamber tapers conically towards the end. Accordingly, a cylindrical–conical separation chamber is applied for the experimental investigations. Thereby, the ratio of the cone length to the total separation chamber length ($L_{\mathrm{CONE}}/L_{\mathrm{SC}}$) is set to 0.53, which results in a cone angle of 5.4°. Additionally, a vortex finder diameter to cyclone diameter ratio of $d_{\mathrm{VF}}/d_{\mathrm{CY^*}} = 0.57$ (see Senn et al. [24]) is ensured to guarantee an optimal operation. As shown in Figure 2, $d_{\mathrm{CY^*}}$ is defined as the diameter of the separation chamber at the location of the vortex finder. Figure 2 provides an exemplary uniflow hydrocyclone prototype with characteristic dimensions. An overview of the geometric parameters used throughout the experimental investigations is given in Table 1.

For evaluating the influence of geometric variations of the particle outlet on the performance of uniflow hydrocyclones, three different particle outlets are designed that differ in the number of particle outlets n_{PO}. Each particle outlet is equipped with nine hydrodynamically shaped guide vanes that consider the least possible influence on the rotating flow, wherefore pressure losses and flow regularities are expected to be small (see Figure 3). The underflow connection is realized via a flexible hose system, which enables a rapid adaption to the used particle outlet geometry. Due to the even arrangement of the hoses, it is ensured that the underflow volume flow rate $\dot{V}_3$ is equally distributed to the particle outlets (see Figure 3).

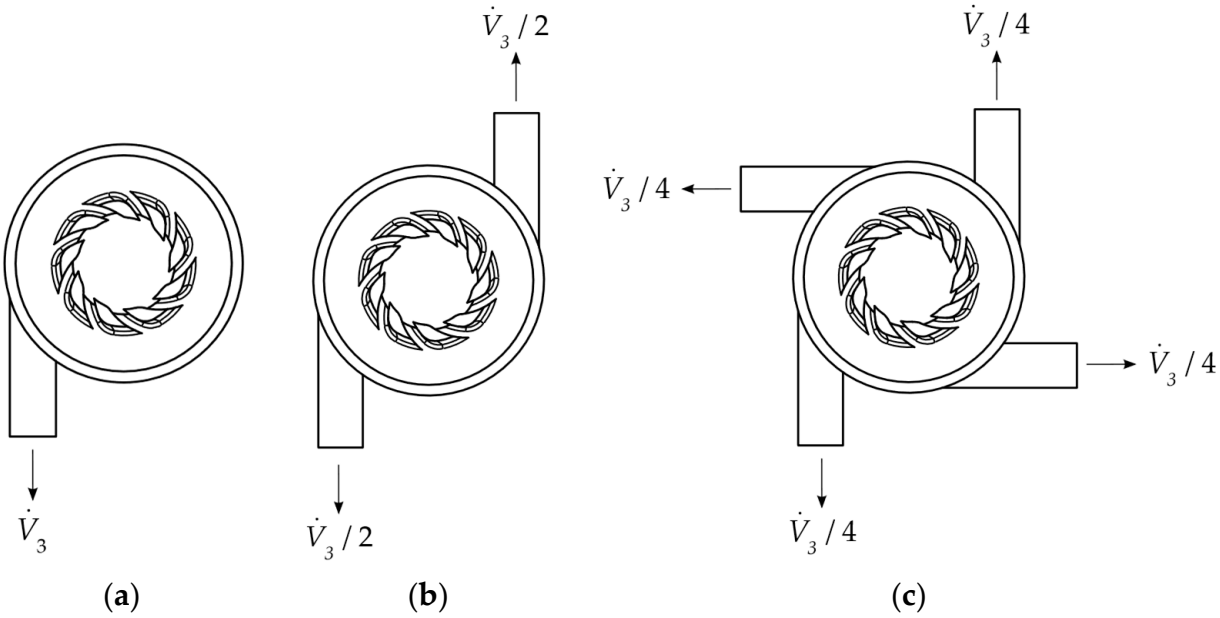

Figure 3. Bottom view of the particle outlet (PO) geometries used for the experimental investigations: (**a**) Single PO; (**b**) Twofold PO; (**c**) Fourfold PO. $\dot{V}_3$ is the underflow volume flow rate.

Additionally, in order to draw far-reaching conclusions about the influence of number of particle outlets on the performance of uniflow hydrocyclones, the experiments are conducted at varying inlet and underflow volume flow rates. Thereby, three different inlet volume flow rates $\dot{V}_1$ (12 $m^3 \cdot h^{-1}$, 15 $m^3 \cdot h^{-1}$ and 18 $m^3 \cdot h^{-1}$) are considered. The magnitude of the underflow volume flow rate is thereby based on the percentage of the inlet volume flow rate, with following underflow to inlet volume flow ratios: $\dot{V}_3 / \dot{V}_1 = 8\%$ and $\dot{V}_3 / \dot{V}_1 = 12\%$.

3. Results and Discussion

For the entirety of the results, the quality criteria specified in Section 2.3. are ensured; therefore, erroneous tests can be excluded. The data points shown in the diagrams (see Figures 4 and 5) correspond to the arithmetic mean value of the obtained results of the respective data sets. For the representation of the separation efficiency, the maximum (upper error bar) and minimum (lower error bar) values are indicated as error bars. In the representation of the pressure drop, error bars are omitted due to negligible deviations. Table 2 provides the justification for neglecting error bars in the representation of the pressure drop for a single particle outlet, an inlet volume flow rate of 12 $m^3 \cdot h^{-1}$ and an underflow to inlet volume flow ratio of 8%.

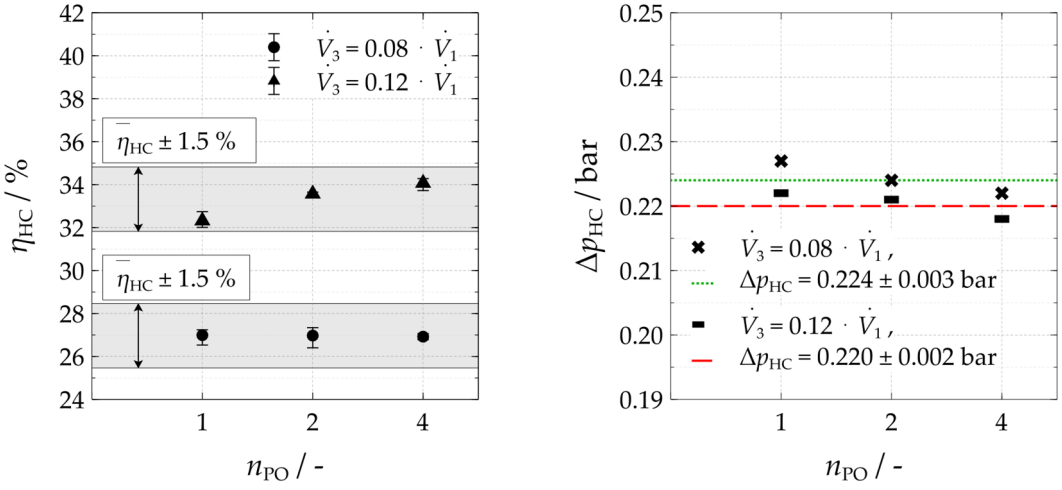

(**a**) Separation efficiency—$\dot{V}_1 = 12$ m³ h⁻¹ (**b**) Pressure drop—$\dot{V}_1 = 12$ m³ h⁻¹

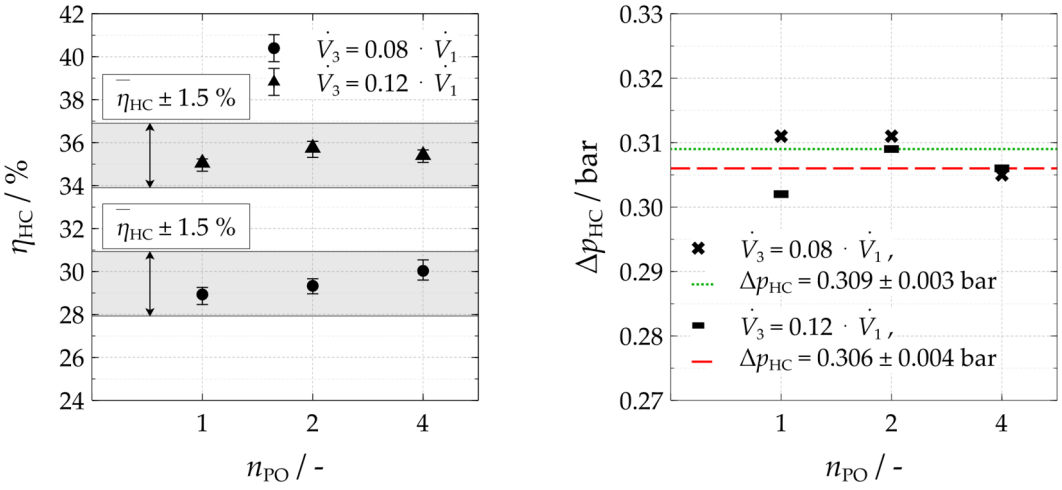

(**c**) Separation efficiency—$\dot{V}_1 = 15$ m³ h⁻¹ (**d**) Pressure drop—$\dot{V}_1 = 15$ m³ h⁻¹

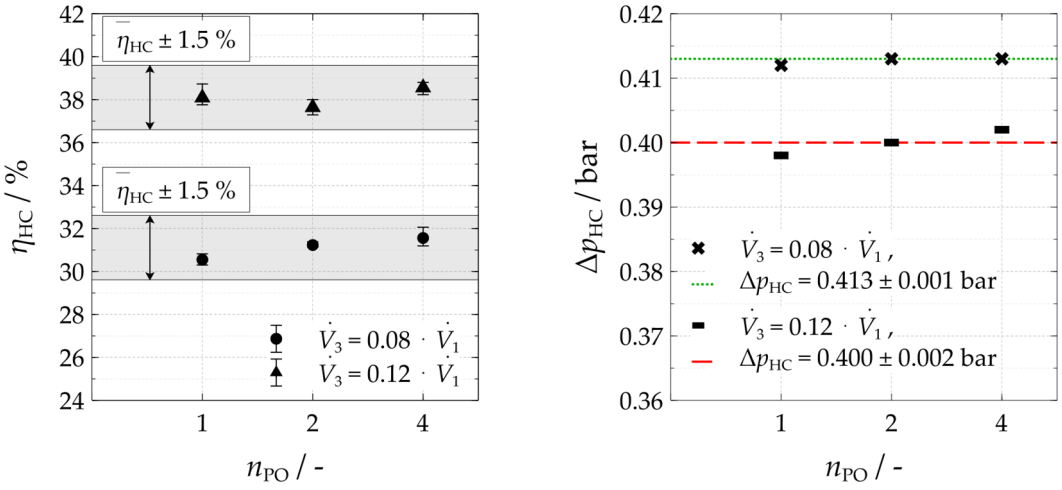

(**e**) Separation efficiency—$\dot{V}_1 = 18$ m³ h⁻¹ (**f**) Pressure drop—$\dot{V}_1 = 18$ m³ h⁻¹

Figure 4. Experimental results for different number of particle outlets n_{PO} for varying inlet and underflow volume flow rates: (**a**,**c**,**e**) Separation efficiency; (**b**,**d**,**f**) Pressure drop. n_{PO}: number of particle outlets, η_{HC}: particle separation efficiency of the hydrocyclone.

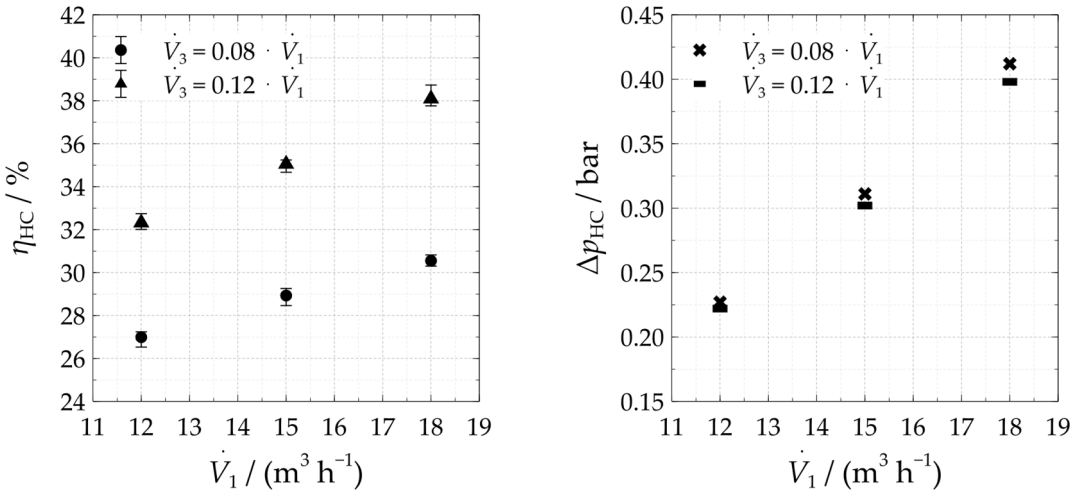

(**a**) Separation efficiency—$n_{PO} = 1$ (**b**) Pressure drop—$n_{PO} = 1$

Figure 5. Experimental results for different inlet and underflow volume flow rates: (**a**) Separation efficiency; (**b**) Pressure drop. η_{HC}: particle separation efficiency of the hydrocyclone.

Table 2. Pressure drops including characteristic quantities for n_{PO} = 1, $\dot{V}_1$ = 12 m^3·h^{-1} and $\dot{V}_3/\dot{V}_1$ = 8%.

Designation	$\Delta p_{HC,\,i}$	Unit
experimental investigation—first revision	0.229	bar
experimental investigation—second revision	0.223	bar
experimental investigation—third revision	0.228	bar
arithmetic mean $\triangleq \Delta p_{HC}$	0.227	bar
range	0.006	bar
standard deviation	0.003	bar

The results of the empirical investigations are shown in Figure 5a–f. First, the results of different particle outlet configurations on separation efficiency are considered. A comparison of the measurement results reveals enhanced separation efficiencies at an increased number of particle outlets for some data series, such as for $\dot{V}_1$ = 12 m^3·h^{-1} and $\dot{V}_3/\dot{V}_1$ = 12% or $\dot{V}_1$ = 15 m^3·h^{-1} and $\dot{V}_3/\dot{V}_1$ = 8%. On the other hand, this trend is contradicted by the experimental data of other datasets (e.g., $\dot{V}_1$ = 18 m^3·h^{-1} and $\dot{V}_3/\dot{V}_1$ = 12%), which impedes an assessment of the influence of the number of particle outlets on the separation performance. For this reason, based on the mean values of the separation efficiencies $\overline{\eta}_{HC}$ of the respective data series, tolerance ranges are included in the diagrams for the presentation of the results. The upper tolerance limit corresponds to $\overline{\eta}_{HC}$ + 1.5%, and the lower tolerance limit to $\overline{\eta}_{HC}$ − 1.5%. These tolerance limits arise from the maximum permissible deviations of the measurement data specified in Section 2.3. The results in Figure 5a,c,e show that the entirety of the experimental results lie within the grey-shaded tolerance ranges ($\overline{\eta}_{HC} \pm 1.5\%$). This holds true for all data points, independent of the inlet and underflow volume flow rates. Hence, it can be inferred that the number of particle outlets does not have a measurable influence on the separation efficiency of uniflow hydrocyclones under the given set of operating conditions. With regard to the separation efficiency, the experimental results leave a large margin for interpretations and can, in the absence of flow profile measurements, hardly be assessed. At the outset, higher separation efficiencies were expected with an increasing number of particle outlets, resulting in a more symmetrical suction and a reduction in the effects of particle backflow described by Weng [25], Kraxner [6] and Senn et al. [24]. As illustrated in Figure 6, this particle backflow effect essentially refers to the fact that particles, which have already been considered to be

separated, are discharged through the overflow due to a backflow in the area of between the vortex finder and the wall of the separation chamber. The assumption that a higher number of particle outlets increases the separation efficiency was based on the fact that the path of particles to the underflow outlets is shortened as n_{PO} increases, which should consequently positively affect the flow conditions in the particle outlet and reduce the extent of recirculation vortices (compare with Oakman and Liow [19]). The results, however, show that the separation efficiency is unaffected by the number of particle outlets. Nonetheless, it needs to be considered that the experimental results are only valid for the specified operating conditions and that a change of the prototype design as well as of the operating and laboratory conditions, would probably lead to different separation characteristics. In this context, particular attention must be paid to the critical loading limit [30] and the properties of the particle collective, which were proven to have a significant influence on the performance of uniflow hydrocyclones. Especially as the separation duration increases, larger particles increase the probability of clogging of the particle outlets [6]. This could be counteracted by an increased number of particle outlets.

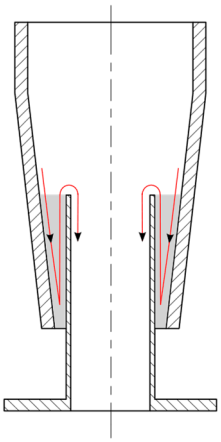

Figure 6. Simplified representation of the particle backflow area.

Additionally, the experimental results show that similarly to the separation efficiency, the pressure drop is also hardly affected by the geometric changes of the particle outlet. To illustrate the minor influences of the number of particle outlets on the pressure drop of uniflow hydrocyclones, the arithmetic mean pressure drops and the pressure drops standard deviations of the respective data series are included in the diagrams ($\Delta p_{HC} \pm \sigma$). The measurement results in Figure 4b,d,f show that by varying the number of particle outlets, maximum standard deviations of the pressure drop of 0.004 bar were recorded throughout the experimental investigations. The minimum standard deviation is only 0.001 bar. Considering the absolute values of the pressure drops, which are in a range of 0.218 bar to 0.413 bar, the obtained standard deviations up to 0.004 bar can be related to sensor uncertainties and are therefore considered negligible. Hence, it can be stated that the pressure drop is independent of the number of particle outlets. Since a uniform distribution of the underflow volume flow rate of the individual particle outlets could be ensured in the experimental investigations (see Figure 3), the pressure loss was expected to be independent of the number of particle outlets. This assumption was reinforced by previous findings, where changes in the pressure drop were mainly attributed to geometric changes of the swirl vane inlet and to the interaction between geometric parameters of the vortex finder and the separation chamber [24]. In the experimental investigations, these influencing parameters were considered constant, wherefore the flow conditions within the uniflow hydrocyclone remained unchanged. At a constant underflow volume flow rate, the volume of particles and water discharged to the underflow per time (flow split ratio) is independent of the number of particle outlets. Accordingly, the volume flow rate, i.e., the flow velocity in the vortex finder, also remains unaffected by variations of the particle

outlet configuration. According to the Bernoulli equation, this results in a constant pressure drop between inlet and overflow duct.

In addition to the influence of the number of particle outlets on the performance of uniflow hydrocyclones, the experimental results in Figure 4 allow one to draw conclusions about the effect of varying inlet and underflow volume flow rates on separation efficiency and pressure drop. The separation efficiency increases with higher inlet volume flow rates $\dot{V}_1$, which is even enhanced at higher underflow volume flow rates $\dot{V}_3$. This can be visualized by plotting the separation efficiency's respective pressure drop over the inlet volume flow rate, which is exemplarily shown for a single particle outlet in Figure 5.

When increasing the inlet volume flow rate from 12 $m^3 \cdot h^{-1}$ to 18 $m^3 \cdot h^{-1}$, separation efficiencies in a range of 26.92% to 31.56% were recorded for a ratio of underflow to inlet volume flow of 8%. As the separation efficiency increases with increasing inlet volume flow rates, an analogy to the operation of reverse-flow hydrocyclones can be derived from the results. Zhang et al. [27] numerically proved that the separation efficiency of reverse-flow hydrocyclones is low at small inlet volume flow rates due to the unsteadiness of the flow field. With increasing inlet volume flow rates, the separation efficiency increases until a threshold value, which is dependent on the geometric properties of the reverse-flow hydrocyclones, is obtained. As the threshold value of the inlet volume flow rate is exceeded, the separation performance decreases due to high negative pressures within the vortex finder. This was also shown by the experimental investigations of Senfter [26]. In the field of uniflow cyclones, this performance behavior was documented by Kraxner [6]. It is therefore evident that such performance characteristics also apply to the operation of uniflow hydrocyclones. Due to the conditions of the test rig and the prototypes, the inlet volume flow rate was limited to 18 $m^3 \cdot h^{-1}$ for the experimental investigations of the current study. The experimental results show that increasing the inlet volume flow rate from 12 $m^3 \cdot h^{-1}$ to 18 $m^3 \cdot h^{-1}$ leads to an increase in separation efficiency. Based on the insights described above, a further increase of $\dot{V}_1$ could, however, lead to a reduction in the separation performance if a critical threshold value is exceeded.

Additionally, by increasing $\dot{V}_3/\dot{V}_1$ to 12%, separation efficiencies up to 38.56% were obtained. Accordingly, increasing ratio of the underflow to inlet volume flow from 8% to 12% ($\triangleq$ increase of 4%) yields an average improvement of the separation efficiency by more than 6%. That higher inlet volume flow rates improve the separation performance is based on principle laws of physics. An increase in $\dot{V}_1$ yields higher tangential velocities and hence centrifugal accelerations that act on the particles. This consequently favors particle separation [5,24]. The gain in separation efficiency at higher underflow to inlet volume flow ratios has already been shown back in 1955 by Sineath [16] and is inevitably related to the increased amount of water and particles drawn into the underflow. Higher underflow volume flow rates consequently lead to higher flow splits, which imply that smaller particles, which would otherwise be discharged in the overflow, are also separated.

With regard to the pressure drop, values in a range of 0.218 bar (with $\dot{V}_1$ = 12 $m^3 \cdot h^{-1}$) to 0.413 bar (with $\dot{V}_1$ = 18 $m^3 \cdot h^{-1}$) were recorded. This increase can be derived from the Bernoulli equation, according to which the pressure drop is proportional to the square of the flow velocity ($\Delta p \propto \vec{v}^2$). Whether there is a quadratic correlation between the inlet volume flow rate and the pressure drop cannot directly be deduced from the results. This is attributable to the fact that the separation tests have only been conducted at three different inlet volume flow rates in a range of 12 $m^3 \cdot h^{-1}$ to 18 $m^3 \cdot h^{-1}$, which limits the scope of observation. In order to reliably prove the quadratic influence, the separation tests should be conducted at an extended range of inlet volume flow rates (e.g., increasing the inlet volume flow rate from 2 $m^3 \cdot h^{-1}$ to 20 $m^3 \cdot h^{-1}$ in equal steps). However, the experimental results additionally show that the increase in pressure drop decreases at higher underflow to inlet volume flow ratios, which was expected due to higher flow split ratios. This results in smaller flow velocities in the overflow and consequently leads to smaller pressure drops.

The observed behavior can again be attributed to the quadratic influence of the flow velocity on the pressure drop.

4. Conclusions

Uniflow hydrocyclones combine a variety of industrially desired properties for solid-liquid separation. To increase the separator's future potential for industrial applications, knowledge on generally valid design criteria, however, indispensably needs to be expanded. Accordingly, the aim of this study was to determine the influence of the number of particle outlets as well as of inlet and underflow volume flow rates on the performance of uniflow hydrocyclones. The results of the empirical investigations showed that a higher number of particle outlets had neither a measurable influence on separation efficiency nor on the pressure drop. Accordingly, a higher number of particle outlets is associated with greater manufacturing effort and complexity without contributing performance enhancements. Therefore, a single particle outlet is preferred under the given set of operating conditions. With regard to the variation in the inlet and underflow volume flow rates, it could be observed that higher volume flow rates favor particle separation but also lead to higher pressure drops. Since higher pressure drops and volume flow rates are related to increased energy expenditures, the choice of the operating conditions should always be made on the basis of a technical-economical analysis.

The results of the experimental investigations provide important new findings in the field of performance influencing parameters of uniflow hydrocyclones. Nonetheless, only selected parameters were considered in the current study, which excludes an encompassing evaluation and indicates that further research is required. In order to improve understanding regarding the flow and separation characteristics, further studies should put increased emphasis on evaluating performance influencing parameters through a combination of experimental and numerical approaches.

Author Contributions: Conceptualization, J.E., T.S. and M.P.; methodology, J.E. and T.S.; software, M.B.; validation, J.E., T.S., M.P. and M.B.; formal analysis, J.E. and M.B.; investigation, J.E., C.M. and T.K.; resources, T.K.; data curation, C.M.; writing—original draft preparation, T.S., J.E. and M.B.; writing—review and editing, M.B., T.S., M.P., C.M. and T.K.; visualization, T.K.; supervision, M.P.; project administration, C.M. All authors have read and agreed to the published version of the manuscript.

Funding: This research received no external funding.

Data Availability Statement: Not applicable.

Conflicts of Interest: The authors declare no conflict of interest.

Appendix A

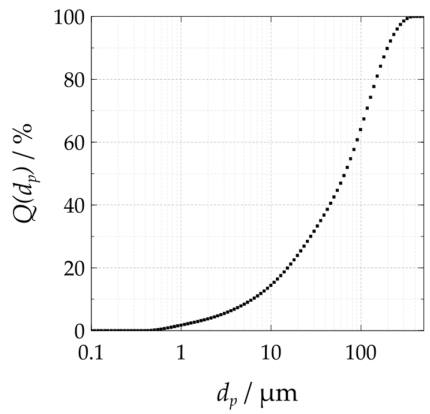

Figure A1. Mass-related cumulative particle size distribution of the used test particles Carolith 0–0.2.

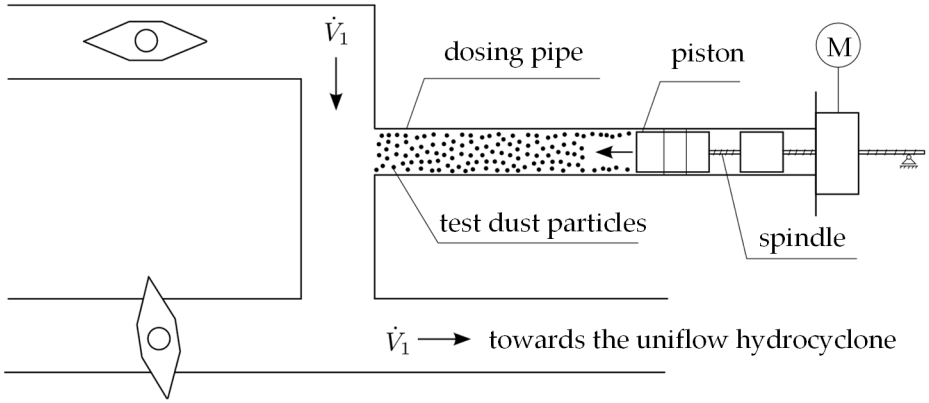

Figure A2. Schematic representation of the motor-driven piston unit.

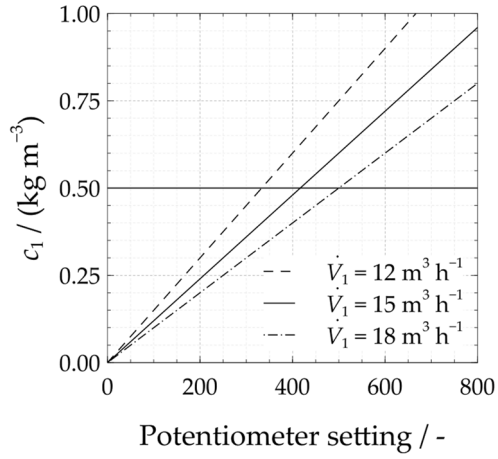

Figure A3. Potentiometer setting for different inlet volume flow rates $\dot{V}_1$.

References

1. Chhabra, R.; Basavaraj, M.G. *Coulson and Richardson's Chemical Engineering: Volume 2A: Particulate Systems and Particle Technology*, 6th ed.; Butterworth-Heinemann: Oxford, UK, 2019; pp. 133–203.
2. Concha, F.A.; Bouse, J.L. *Fluid Mechanics Fundamentals of Hydrocyclones and Its Applications in the Mining Industry*; Springer: Cham, Switzerland, 2021; pp. 1–8.
3. Muschelknautz, U. Design criteria for multicyclones in a limited space. *Powder Technol.* **2019**, *357*, 2–20. [CrossRef]
4. Pillei, M.; Kofler, T.; Wierschem, A.; Kraxner, M. Intensification of uniflow cyclone performance at low loading. *Powder Technol.* **2020**, *360*, 522–533. [CrossRef]
5. Liow, J.L.; Oakman, O.A. Performance of mini-axial hydrocyclones. *Miner. Eng.* **2018**, *122*, 67–78. [CrossRef]
6. Kraxner, M. Empirische Ermittlung von Auslegungskriterien für Gleichstromzyklone in Multizyklonblöcken. Ph.D. Thesis, Technische Universität München, Munich, Germany, 2012.
7. Gauthier, T.A.; Briens, C.L.; Bergougnou, M.A.; Galtier, P. Uniflow cyclone efficiency study. *Powder Technol.* **1990**, *62*, 217–225. [CrossRef]
8. Tan, Z.; Zhang, H.; Abedi, J.; Yu, Z.; Martinuzzi, R. Development of a new high-efficiency simple structure cyclone. *Can. J. Chem. Eng.* **2009**, *87*, 343–349. [CrossRef]
9. Oh, J.; Choi, S.; Kim, J.; Lee, S.; Jin, G. Particle separation with the concept of uniflow cyclone. *Powder Technol.* **2014**, *254*, 500–507. [CrossRef]
10. Nieuwstadt, F.T.M.; Dirkzwager, M. A fluid mechanics model for an axial cyclone separator. *Ind. Eng. Chem. Res.* **1995**, *34*, 3399–3404. [CrossRef]
11. Delfos, R.; Murphy, S.; Stanbridge, D.; Olujic, Z.; Jansens, P.J. A design tool for optimising axial liquid-liquid hydrocyclones. *Miner. Eng.* **2004**, *17*, 721–731. [CrossRef]
12. Liu, M.; Chen, J.; Cai, X.; Han, Y.; Xiong, S. Oil-water pre-separation with a novel axial hydrocyclone. *Chin. J. Chem. Eng.* **2018**, *26*, 60–66. [CrossRef]
13. Hamza, J.E.; Al-Kayiem, H.H.; Lemma, T.A. Experimental investigation of the separation performance of oil/water mixture by compact conical axial hydrocyclone. *Therm. Sci. Eng. Prog.* **2020**, *17*, 100358. [CrossRef]

14. Al-Kayiem, H.H.; Hamza, J.E.; Lemmu, T.A. Performance enhancement of axial concurrent liquid-liquid hydrocyclone separator through optimization of the swirler vane angle. *J. Pet. Explor. Prod. Technol.* **2020**, *10*, 2957–2967. [CrossRef]
15. Kou, J.; Jiang, Z.; Cong, Y. Separation characteristics of an axial hydrocyclone separator. *Processes* **2021**, *9*, 2288. [CrossRef]
16. Sineath, H.H. Operation Characteristics of Fixed-Impeller Hydrocyclones. Ph.D. Thesis, Georgia Institute of Technology, Atlanta, GA, USA, 1955.
17. Sineath, H.H.; Della Valle, J.M. Fixed impeller hydrocyclones. *Chem. Eng. Prog.* **1959**, *55*, 59–65.
18. Ogawa, A.; Suzuki, T. Theory of the cut-size, the fractional collection efficiency, and the vortex breakdown in the axial flow hydro-cyclone. *Part. Sci. Technol.* **2001**, *19*, 257–299. [CrossRef]
19. Oakman, O.A.; Liow, J.L. Simulation and Experimental Validation of an Axial-Flow Hydrocyclone. In Proceedings of the 20th Australasian Fluid Mechanics Conference, Perth, Australia, 5–8 December 2016.
20. Niazi, S.; Habibian, M.; Rahimi, M. Performance evaluation of a uniflow mini-hydrocyclone for removing fine heavy metal particles from water. *Chem. Eng. Res. Des.* **2017**, *126*, 89–96. [CrossRef]
21. Murphy, S.; Delfos, R.; Pourquie, M.J.B.M.; Olujic, Z.; Jansens, P.J.; Nieuwstadt, F.T.M. Prediction of strongly swirling flow within an axial hydrocyclone using two commercial CFD codes. *Chem. Eng. Sci.* **2007**, *62*, 1619–1635. [CrossRef]
22. Rocha, A.D.; Bannwart, A.C.; Ganzarolli, M.M.; Quintella, E.F. Numerical study of swirling flow in a liquid-liquid axial hydrocyclone separator. In Proceedings of the 20th International Congress of Mechanical Engineering, Gramado, Brazil, 15–20 November 2009.
23. Mokni, I.; Dhaouadi, H.; Bournot, P.; Mhiri, H. Numerical investigation of the effect of the cylindrical height on separation performances of uniflow hydrocyclone. *Chem. Eng. Sci.* **2015**, *122*, 500–513. [CrossRef]
24. Senn, M.; Berger, M.; Senfter, T.; Pillei, M.; Kraxner, M. Empirical and Numerical Investigation of an Uniflow Hydrocyclone. In Proceedings of the 15th Minisymposium Chemical and Process Engineering and 6th Austrian Particle Forum, Leoben, Austria, 29–30 April 2019.
25. Weng, M. Experimentelle und Numerische Untersuchung von Gleichstromhydrozyklonen. Ph.D. Thesis, Technische Hochschule Aachen, Aachen, Germany, 2002.
26. Senfter, T. Kontinuierliche Störstoffabscheidung in der Klärschlamm-Co-Fermentation Mittels Zentrifugalabscheider. Ph.D. Thesis, Universität Innsbruck, Innsbruck, Austria, 2018.
27. Zhang, C.; Cui, B.; Wei, D.; Zhao, Q.; Luo, N.; Feng, Y. Predicting the optimum range of feed flow rate in a hydrocyclone using the method combined flow pattern and equation model. *Powder Technol.* **2017**, *319*, 279–288. [CrossRef]
28. Cui, B.; Zhang, C.; Zhao, Q.; Hou, D.; Wie, D.; Song, T.; Feng, Y. Study on interaction effects between the hydrocyclone feed flow rate and the feed size distribution. *Powder Technol.* **2020**, *366*, 617–628. [CrossRef]
29. *ISO 5011:2020*; Inlet Air Cleaning Equipment for Internal Combustion Engines and Compressors—Performance Testing. International Organization for Standardization: London, UK, 2020.
30. Pillei, M. Optimierung von Gleichstromzyklonen bei Geringer Feststoffbeladung. Ph.D. Thesis, Friedrich-Alexander-Universität, Erlangen, Germany, 2020.